

Fundamental Limits of Rigid Body Localization

Niclas Führling[Ⓢ], *Graduate Student Member, IEEE*, Ivan Alexander Morales Sandoval[Ⓢ], *Graduate Student Member, IEEE*, Giuseppe Thadeu Freitas de Abreu[Ⓢ], *Senior Member, IEEE*, Gonzalo Seco-Granados[Ⓢ], *Fellow, IEEE*, David González G.[Ⓢ], *Senior Member, IEEE*, and Osvaldo Gonsa[Ⓢ]

Abstract—We consider a novel and general approach to easily compute the Cramér-Rao Lower Bounds (CRLBs) of rigid body localization (RBL) problem using arbitrary types of information. To that end, we adopt an information-centric construction of the Fisher information matrix (FIM), which allows capturing the contribution of each measurement towards the FIM explicitly, both in terms of input measurement types, as well as of their error distributions. Taking advantage of this approach, we derive a generic framework for evaluating the CRLB, which is applicable to arbitrary rigid body localization scenarios, and which, unlike the formulation of FIM commonly used in point-target localization, is better suited to RBL problems as it explicitly allows capturing the precision in both the translation vector and the rotation matrix (or alternative the rotation angles) of the rigid body, with respect to a reference. Examples of CRLBs obtained via the proposed approach are given in closed form, including the bound incorporating an orthonormality constraint onto the rotation matrix, which enables a straightforward adjustment of the derived bound when new measurements are added or removed. Numerical results illustrate that the derived expression correctly lower-bounds the errors of estimated localization parameters obtained via various related state-of-the-art (SotA) estimators, revealing their accuracies and suggesting that SotA RBL algorithms can still be improved.

Index Terms—Rigid Body Localization, Cramér Rao Lower Bound, Fisher Information.

I. INTRODUCTION

LOCALIZATION algorithms are of great interest in wireless system applications such as autonomous driving [1], robotics [2], augmented reality [3], internet of vehicles (IoV) [4] and digital twins [5], which implies that understanding the limits of their performance is of essential importance to determining the feasibility of such applications. The most prominent of these bounds is the Cramér-Rao Lower Bound (CRLB), which provides a fundamental limit on the variance of unbiased estimates of a given parameter [6], applicable not only in the context of localization [7], but also in many other fields, such as machine learning [8], radar systems [9], and communications [10]. The CRLB is derived from the Fisher information matrix (FIM), which captures the amount of information that a set of measurements provides about the parameters of interest. Although other well known bounds such as the Bhattacharyya bound [11], the Hodges-Lehmann bound [12] or the Weiss-Weinstein bound [13] also exist, the CRLB is the most widely used in the literature, as it is relatively easy to compute compared to more complex bounds.

N. Führling, I. A. Morales Sandoval and G. T. F. de Abreu are with the School of Computer Science and Engineering, Constructor University, Campus Ring 1, 28759, Bremen, Germany (e-mails: [nfuehrling, imorales, gabreu]@constructor.university).

G. Seco-Granados is with the Department of Telecommunications and Systems Engineering, Universitat Autònoma de Barcelona, Spain (email: gonzalo.seco@uab.cat).

D. González G. and O. Gonsa are with AUMOVIO Germany GmbH, Guerickestrasse 7, 60488, Frankfurt am Main, Germany (e-mail: david.gonzalez.g@ieee.org, osvaldo.gonsa@aumovio.com).

Wireless localization [14]–[16] can be seen as an early example of integrated sensing and communications (ISAC), in so far as it demonstrates how communication signals can be repurposed to acquire situational awareness, which is increasingly seen as a key added value of beyond fifth-generation (B5G) [17] and sixth-generation (6G) [18] systems, as recent advancements in ISAC technology [19], [20] have indeed shown that radar parameters (*i.e.*, range, bearing and velocity) can be extracted from conventional communications signals [9], [21]. This can be done both actively, *i.e.*, via signals transmitted by the target, or passively, *i.e.*, via round-trip reflections of signals transmitted by the sensors themselves, resulting in richer and more abundant positioning information.

As a result of the above, there is growing interest in the rigid body localization (RBL) problem [22]–[24], which extends beyond single-point localization towards systems capable of inferring not only the location of point targets, but also the shape and orientation of extended targets represented by a set of pre-defined landmark points. However, in spite of the vast variety of approaches and state-of-the-art (SotA) algorithms to solve the rigid body localization (RBL) problem [25]–[29], a generic bound on the accuracy parameter estimates applicable to any type of RBL scenario has not yet appeared, which is a key requirement for the design of robust localization systems and the corresponding evaluation of their performance.

In order to obtain the CRLB for any estimation problem, a corresponding FIM needs to be constructed, which is based on the probability density function (PDF) of the associated measurements, calculated by taking the expected value of the negative second derivative of the log-likelihood function with respect to the parameter vector that captures the amount of information that the observed data carries about the parameters. This is a well known and widely used approach in the literature, which will be hereafter referred to as the *element-centric* FIM formulation [6].

In light of this approach, many works have derived CRLBs for specific localization applications. For instance, low earth orbit (LEO)-based localization was considered in [30], while holographic positioning was addressed in [31]. Bounds under other scenarios and for various applications have also been derived, *e.g.*, in [32]–[36]. These works provide valuable insights into the performance limits of specific localization scenarios, however, they do not offer a general framework for deriving the CRLB for the RBL problem specifically.

The key distinction between RBL and the more conventional and widely studied point-target localization is that in RBL the landmark points defining a given three-dimensional (3D) object are rigidly “locked” together, such that instead of the location of the landmark points themselves, one is interested in estimating the translation and rotation parameters of the rigid body, relative to a known prior reference position.

It follows that bounding the errors of RBL algorithms via the CRLB approach requires the evaluation of FIMs that explicitly capture the precision of these parameters, rather than the location of the landmark points individually. This requirement when deriving RBL-specific CRLB has been partially addressed in related literature, but only for certain scenarios and under limited types or observations and error models. For instance, a unitarily constrained CRLB for the 3D RBL case was derived in [28], but for the range-based estimation case only, and under the assumption that measurement errors are Gaussian. In turn, in [37], unconstrained CRLBs with generic measurement covariances were derived for stationary and moving 2D RBL problems, while the constrained 3D case was only briefly discussed, without being fully addressed. Besides the aforementioned limitations, the CRLBs given in [28] and [37] have in common the standard element-centric approach to constructing the FIM, whereby each of its entry is obtained with basis on the entire likelihood function of all observations under the whole set of desired estimate parameters, which can be very cumbersome to evaluate, especially when dealing with complex scenarios involving multiple types of measurements and error distributions.

To the best of our knowledge, no general and comprehensive approach to compute CRLBs for RBL problems have yet been given, which is the goal of this article. In so doing, we shall also build on a modern approach to constructing FIM [38], whereby each input measurement, as well as the corresponding type of error, is accounted for independently¹. Such an approach, here referred to as the *information-centric* FIM formulation, defines the FIM in a sum-product form that can be applied and extended to any type of localization scenario, including the RBL problem.

All in all, we propose in this article a novel formulation of the CRLB suitable to RBL, namely, aimed at determining the fundamental limit on the estimate of the translation and the rotation of a rigid body relative to a given reference position. To that extend, we first revisit the original information-centric FIM formulation for a target group of independent nodes [38], which is then extended to the case of a rigid body, evaluating it with respect to the rotation and translation parameters by making use of the simple sum-product formulation of the FIM. The proposed CRLB expression can be applied to any type of rigid body localization scenario, where we additionally provide the closed-form expressions for specific case of the constrained bound for the rotation matrix, since the rotation matrix is part of the special orthogonal group.

The contributions of this article are summarized as follows:

- Leveraging an information-centric approach to constructing the FIM [38], a novel general framework to obtain CRLBs for RBL is derived, which captures the fundamental limits of the estimates of translation and rotation angles of rigid bodies, relative to a reference position.
- Closed-form expressions for the derived CRLBs are offered for multiple measurement types and error distributions, which can be directly applied to any RBL scenario

¹This assumes, of course, that measurements are obtained independently, which however is the case in the vast majority of real-life applications, and which in any case yields an absolute limit.

and enable a straightforward calculation of the bounds if new measurements are added or removed.

- Addressing the orientation estimation further, a variation of the latter bound is also derived for the case where the entire rotation matrix, rather than individual angles, is obtained, where the rotation matrix is constrained to be in the special orthogonal group.

The remainder of the article is organized as follows. First, a description of the rigid body representation and a description of the information-centric FIM formulation are offered in Section II. Then, in Section III, the proposed derivation of the CRLBs for the parameters estimated in RBL problems is explained. Finally, a numerical evaluation of the proposed bounds is presented in Section IV, along with comparisons with various related SotA RBL algorithms. Conclusions and some words on possible future work then follow in Section V, and some additional material aimed at facilitating understanding of some the work are offered in Appendices.

II. PRELIMINARIES

A. Rigid Body Representation Model

Before proceeding with the proposed CRLB derivation, we first introduce the RBL system model and information-centric FIM formulation which sets the basis of subsequent derivations. To that extend, let us refer to Figure 1 and consider an arbitrary rigid body in the 3D space, that can be represented by a collection of N landmark points $\mathbf{c}_n \in \mathbb{R}^{3 \times 1}$, with $n = \{1, \dots, N\}$, such that the corresponding conformation matrix \mathbf{C} describing the shape of the body is constructed by the column-wise collection of the individual landmark position vectors \mathbf{c}_n , *i.e.*, $\mathbf{C} \triangleq [\mathbf{c}_1, \dots, \mathbf{c}_N] \in \mathbb{R}^{3 \times N}$.

As also illustrated in Figure 1, let Θ be the location of said transformed rigid body relative to the conformation matrix \mathbf{C} , be given by the following linear transformation of the latter

$$\Theta = \mathbf{Q} \cdot \mathbf{C} + \mathbf{t} \cdot \mathbf{1}_N^T, \quad (1)$$

where $\mathbf{t} \in \mathbb{R}^{3 \times 1}$ is a translation vector given by the distance between the geometric center (centroid) of the body and the centroid in the corresponding reference frame, $\mathbf{1}_N$ is a column vector with N entries all equal to 1, and $\mathbf{Q} \in \mathbb{R}^{3 \times 3}$ is a rotation matrix², determined by the corresponding yaw, pitch and roll angles α, β and γ , respectively, namely

$$\begin{aligned} \mathbf{Q} &\triangleq \mathbf{Q}_z(\gamma) \mathbf{Q}_y(\beta) \mathbf{Q}_x(\alpha) \\ &= \begin{bmatrix} \cos \gamma & -\sin \gamma & 0 \\ \sin \gamma & \cos \gamma & 0 \\ 0 & 0 & 1 \end{bmatrix} \cdot \begin{bmatrix} \cos \beta & 0 & \sin \beta \\ 0 & 1 & 0 \\ -\sin \beta & 0 & \cos \beta \end{bmatrix} \cdot \begin{bmatrix} 1 & 0 & 0 \\ 0 & \cos \alpha & -\sin \alpha \\ 0 & \sin \alpha & \cos \alpha \end{bmatrix} \\ &= \begin{bmatrix} \cos \beta \cos \gamma \sin \alpha \sin \beta \cos \gamma - \cos \alpha \sin \gamma \cos \alpha \sin \beta \cos \gamma + \sin \alpha \sin \gamma \\ \cos \beta \sin \gamma \sin \alpha \sin \beta \sin \gamma + \cos \alpha \cos \gamma \cos \alpha \sin \beta \sin \gamma - \sin \alpha \cos \gamma \\ -\sin \beta & \sin \alpha \cos \beta & \cos \alpha \cos \beta \end{bmatrix} \\ &= \begin{bmatrix} q_{1,1} & q_{1,2} & q_{1,3} \\ q_{2,1} & q_{2,2} & q_{2,3} \\ q_{3,1} & q_{3,2} & q_{3,3} \end{bmatrix}. \end{aligned} \quad (2)$$

²The rotation matrix \mathbf{Q} is part of the special orthogonal group such that $SO(3) = \{\mathbf{Q} \in \mathbb{R}^{3 \times 3} : \mathbf{Q}^T \mathbf{Q} = \mathbf{I}, \det(\mathbf{Q}) = 1\}$ [39], which is interpreted as estimating of the 9 elements of the corresponding rotation matrix \mathbf{Q} as a whole. However, as shown in [40], [41] this representation can be extended by replacing the estimation of \mathbf{Q} with the estimation of the associated and fundamental yaw, pitch and roll angles (α, β, γ) .

As should be clear from equation (1), the translation vector that describes the motion of rigid body from \mathcal{C} to Θ is given by the vector defined by the centroids of the body at those locations. But since the centroid of any collection of points is uniquely defined, the same principle can be used to define the translation vector \mathbf{t} more generally. Consider therefore the scenario illustrated in Figure 2, where a target rigid body is to be localized by a set of anchor nodes³, whose locations are assumed to be known. For the sake of exposition, the set of anchors can be treated as a second rigid body, such that one can speak of two distinct rigid bodies hereafter referred to by their indices $i = \{1, 2\}$, which generally have different shapes and/or are characterized by generally distinct numbers n_T and n_A of landmark points, respectively. It follows that, under a common absolute reference frame, the two bodies can be represented by the corresponding distinct conformation matrices $\mathbf{C}_1 \in \mathbb{R}^{3 \times n_T}$ and $\mathbf{C}_2 \in \mathbb{R}^{3 \times n_A}$, with $\mathbf{C}_i = [\mathbf{c}_{i,1}, \dots, \mathbf{c}_{i,N_i}] \in \mathbb{R}^{3 \times N_i}$, where $\mathbf{c}_{i,n}$ is the location of the n -th point of the i -th body.

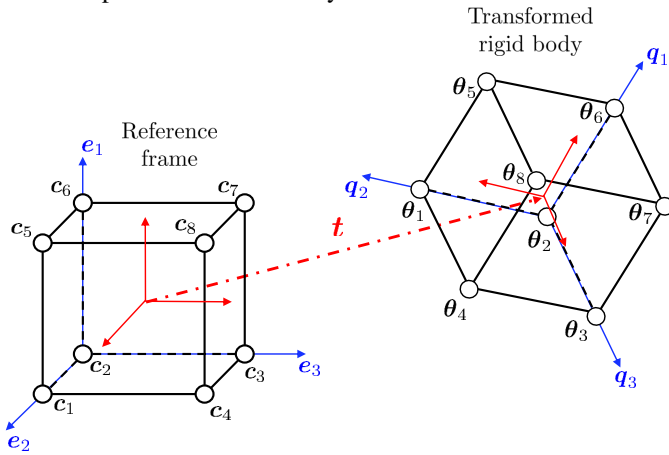


Fig. 1. Illustration of a rigid body at an initial location aligned with a reference frame \mathcal{C} , and at another location Θ , as obtained after the linear transformation described in equation (1), comprising a 3D rotation via the matrix \mathbf{Q} and a translation by the vector \mathbf{t} . Notice that by force of the latter, the rotation matrix \mathbf{Q} reduces to an identity $\mathbf{I} = [\mathbf{e}_1, \mathbf{e}_2, \mathbf{e}_3]$ if the body is at its canonic location such that $\Theta = \mathcal{C}$.

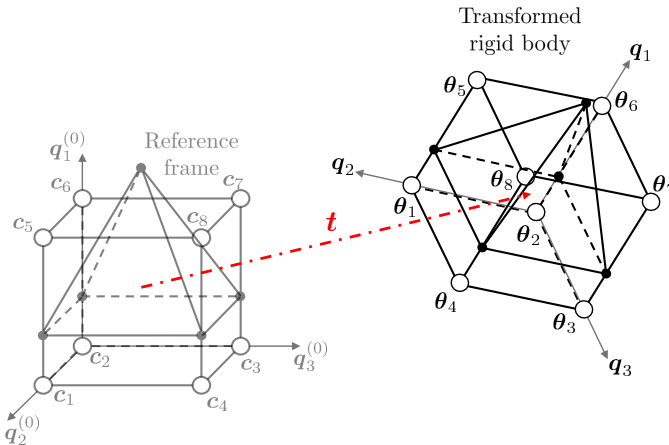


Fig. 2. Illustration of a scenario where a rigid body with $n_A = 5$ landmark points seeks to locate another rigid body with $n_T = 8$ points.

³Without loss of generality, we will refer to the target body as the first body, and the set of anchors as the second body, where the second body containing the anchor nodes can either be assumed to be multiple nodes of a positioning infrastructure [37], or an actual second rigid body that egoistically seeks to locate the first [42], without any knowledge about the target's conformation.

It is worth emphasizing that the location and orientation of one body relative to another can still be modeled by equation (1), although in general scenarios the two rigid bodies are not identical, such that $\mathcal{C}_1 \neq \mathcal{C}_2$, in the sense that the following still holds

$$\Theta_i = \mathbf{Q} \cdot \mathbf{C}_i + \mathbf{t} \cdot \mathbf{1}_{N_i}^T, \forall i \in \{1, 2\}, \quad (3)$$

where the same rotation matrix \mathbf{Q} and translation vector \mathbf{t} is used for both $i \in \{1, 2\}$, as illustrated in Figure 2.

B. Fisher Information Matrix Construction Framework

In light of the above, we hereafter consider a general scenario in which two distinct rigid bodies, hereafter referred to by their indices $i = \{1, 2\}$, have different shapes and/or are characterized by distinct numbers n_T and n_A of landmark points, such that there are $N = n_T + n_A$ landmark points in total. Consequently, the indices of the rigid bodies landmark points can be referred to as a target group $\mathcal{T} = \{1, \dots, t, \dots, n_T\}$ and an anchor group $\mathcal{A} = \{1, \dots, a, \dots, n_A\}$, respectively, such that the coordinates of the target and anchor groups are represented by the corresponding rigid body conformation matrices, which can be written as $\Theta_{\mathcal{T}} \in \mathbb{R}^{3 \times n_T}$ and $\Theta_{\mathcal{A}} \in \mathbb{R}^{3 \times n_A}$, respectively.

The fundamental limits of RBL depend on the both type of measurements available and the corresponding errors affecting them, where we emphasize that the type of measurements (distances, angles, etc.) relates to the geometry of the estimation problem, while the measurement errors relates to the statistical uncertainty over the latter quantities. It will prove convenient, therefore, to separate these two distinct aspects of the input. To that end, let us start by defining a mapping function that captures the dissimilarity between any arbitrary target point n and reference anchor node a , which is given by

$$g(\theta_n | \theta_a) : \mathbb{R}^\eta \rightarrow \mathbb{R}, \quad (4)$$

where η is the dimension of the target and anchor nodes coordinates θ_n and θ_a .

We shall refer to the mapping function $g(\theta_n | \theta_a)$ as the *dissimilarity function*, since it yields a measure of dissimilarity between a target node and anchor node. The acquired values of the dissimilarity measurements are, however, typically subject to errors, such that we also introduce the corresponding probability density function, hereafter referred to as the *variation function*, which is denoted by $p_{na}(r_{na}; g(\theta_n | \theta_a))$, where r_{na} is the random variable associated with the measured dissimilarity between the target point t and anchor node n .

Some examples of point-target dissimilarity functions are given in Table I, with a few corresponding suitable variation functions for different error models given in Table II.

In possession of a given dissimilarity and variation function associated with the Fisher information between target t and anchor n given the variates r_{na} , is described by [6]

$$F_{na} = \mathbb{E}_{r_{na}} \left[\left(\frac{\partial \ln p_{na}(r_{na}; g(\theta_n | \theta_a))}{\partial g(\theta_n | \theta_a)} \right)^2 \right], \quad (5)$$

where $\mathbb{E}[\cdot]$ denotes the expectation operator, applied to the gradient of the log-likelihood function with respect to the dissimilarity function $g(\theta_n | \theta_a)$.

TABLE I
DISSIMILARITY FUNCTIONS AND INFORMATION GRADIENTS IN POINT-TARGET WIRELESS LOCALIZATION SYSTEMS.

Measure Type	Dissimilarity Function $g(\theta_n \theta_a)$	Information Gradient $\mathbf{v}_{na} = \nabla_{\theta} g(\theta_n \theta_a)$
Distance	$g(\theta_n \theta_a) = \ \theta_n - \theta_a\ = d_{na}$	$\frac{\partial g(\theta_n \theta_a)}{\partial \theta_n} = \frac{1}{\ \mathbf{d}_{na}\ } [(x_t - x_n), (y_t - y_n), (z_t - z_n)]^T = \frac{\mathbf{d}_{na}}{d_{na}}$
Angle of Arrival	$g(\theta_n \theta_a; \{\mathbf{a}, \mathbf{b}\}) = \arccos\left(\frac{\langle \mathbf{d}_{na}, \mathbf{b} \rangle}{\ \mathbf{d}_{na}\ \ \mathbf{b}\ }\right)$	$\frac{\partial g(\theta_n \theta_a)}{\partial \theta_n} = \frac{1}{\ \mathbf{d}_{na}\ ^2} [(y_t - y_n), -(x_t - x_n), 0]^T = \begin{bmatrix} 0 & 1 & 0 \\ -1 & 0 & 0 \\ 0 & 0 & 0 \end{bmatrix} \frac{\mathbf{d}_{na}}{d_{na}^2}$
Angle Difference of Arrival	$g(\theta_n \theta_a, \theta_k) = \arccos\left(\frac{d_{na}^2 + d_{ka}^2 - d_{nk}^2}{2d_{na}d_{ka}}\right)$	$\frac{\partial g(\theta_n \theta_a, \theta_k)}{\partial \theta_n} = \frac{d_{na}}{\ \mathbf{d}_{nk} \times \mathbf{d}_{na}\ } (\rho_1 \mathbf{d}_{na} + \rho_2 \mathbf{d}_{nk})$

* Notes: a) The coordinate vectors are explicitly written as $\theta_a \triangleq [x_n, y_n, z_n]^T$ and $\theta_n \triangleq [x_t, y_t, z_t]^T$; b) The distance vector between θ_n and θ_a is defined as $\mathbf{d}_{na} \triangleq \theta_n - \theta_a$; c) The notation $\langle \cdot, \cdot \rangle$ denotes the inner product between two vectors; d) The unit-norm vector \mathbf{a} , centered at θ_a and belonging to a reference plane for angle-of-arrival measurements; and e) The unit-norm vector \mathbf{b} , also centered at θ_a and belonging to the latter plane, is a reference vector against which the angle of arrival is measured (see Figure 5); e) The coefficients $\rho_1 \triangleq \frac{d_{ka}^2 - (d_{na}^2 + d_{nk}^2)}{2d_{ka}d_{na}}$ and $\rho_2 \triangleq \frac{1}{d_{ka}}$.

TABLE II
INFORMATION INTENSITIES FOR DIFFERENT VARIATION FUNCTIONS

Model	Variation Function $p(r_{na}; g(\theta_n \theta_a))$	Information Intensity \sqrt{F}	Reference
Normal	$p(r_{na}; g(\theta_n \theta_a)) = \mathcal{N}(g(\theta_n \theta_a), \sigma^2)$	$\sqrt{F} = \frac{1}{\sigma}$	[43]
Normal with $\sigma^2 = \beta(g(\theta_n \theta_a))^{\alpha^1}$	$p(r_{na}; g(\theta_n \theta_a)) = \mathcal{N}(g(\theta_n \theta_a), \beta(g(\theta_n \theta_a))^{\alpha})$	$\sqrt{F} = \sqrt{\frac{1}{\beta(g(\theta_n \theta_a))^{\alpha}} + \frac{\alpha^2}{2(g(\theta_n \theta_a))^2}}$	[44]
Von-Mises	$p(r_{na}; g(\theta_n \theta_a)) = \frac{\exp(\omega \cos(r_{na} - g(\theta_n \theta_a)))}{2\pi I_0(\omega)}$	$\sqrt{F} = \frac{\omega}{\sqrt{2}}$	Appendix A-A
Nakagami- m with controlling spread Υ^2	$p(r_{na}; g(\theta_n \theta_a)) = \frac{2m^m}{\Gamma(m)\Upsilon^m} r_{na}^{2m-1} \exp\left(-\frac{m}{\Upsilon} r_{na}^2\right)$	$\sqrt{F} = \sqrt{\frac{m(4m-3)}{\Upsilon(m-1)}}$	Appendix A-B
Gamma with shape and scale parameter κ and v^3	$p(r_{na}; g(\theta_n \theta_a)) = \frac{1}{\Gamma(\kappa)v^{\kappa}} r_{na}^{\kappa-1} \exp\left(-\frac{r_{na}^2}{v}\right)$	$\sqrt{F} = \sqrt{\frac{1}{v^2(\kappa-2)}}$	Appendix A-C

¹ Here α is the pathloss exponent, while β is a scaling factor related to the sensitivity of the transmitter.

² Here $m \geq \frac{1}{2}$ and $\Upsilon > 0$ are the shape and spread control parameters.

³ Here $\kappa > 0$ and $v > 0$ are the shape and scale parameter.

Taking into account all pairs of target point and anchor node, collected in the set $\mathcal{P} \triangleq \{(n, a), \forall n \text{ and } \forall a\}$, the likelihood function corresponding to all target points is the group $\Theta_{\mathcal{T}}$ can then be given by

$$\mathcal{L}(\mathbf{r}|\Theta_{\mathcal{T}}) = \prod_{(n,a) \in \mathcal{P}} p_{na}(r_{na}; g(\theta_n|\theta_a)), \quad (6)$$

where \mathbf{r} is the vector of all independent measurements, and $\Theta_{\mathcal{T}}$ is the vector of all target coordinates.

Collecting the expression above for all target points, the FIM can be constructed as

$$\mathbf{F}_{\Theta_{\mathcal{T}}} = \mathbb{E}[\nabla_{\Theta_{\mathcal{T}}} \ln(\mathcal{L}(\mathbf{r}|\Theta_{\mathcal{T}})) \nabla_{\Theta_{\mathcal{T}}}^T \ln(\mathcal{L}(\mathbf{r}|\Theta_{\mathcal{T}}))], \quad (7)$$

where $\nabla_{\Theta_{\mathcal{T}}}$ is the gradient operator with respect to the target coordinates $\Theta_{\mathcal{T}}$.

We refer to the FIM construction directly via equation (7) as *element-centric*, since in this case the matrix $\mathbf{F}_{\Theta_{\mathcal{T}}}$ is obtained on an element-by-element basis from equation (5), and remark that although this usual approach to construct the FIM is concise mathematically, it is not very insightful in elucidating the contribution of each measurement towards knowledge on the parameters to be estimated.

In contrast, we revise in the sequel an alternative approach to construct FIMs [38] in which $\mathbf{F}_{\Theta_{\mathcal{T}}}$ is obtained by a sum of

rank-one matrices, each carrying the contribution of only one measurement between an anchor node a and a target point n , of whatever type.

Lemma 1 (Sum-product Formulation of FIM). *Consider the unbiased estimation of the parameters of interest in $\Theta_{\mathcal{T}}$ from the input vector \mathbf{r} with the associated dissimilarity function $g(\theta_n|\theta_a)$ and variation function $p_{na}(r_{na}; g(\theta_n|\theta_a))$, where $n \in \{1, \dots, n_{\mathcal{T}}\}$ and $a \in \{1, \dots, N\}$. Then the FIM $\mathbf{F}_{\Theta_{\mathcal{T}}}$ can be obtained in an information-centric approach from the sum of information vector products [45]:*

$$\mathbf{F}_{\Theta_{\mathcal{T}}} = \sum_{(n,a) \in \mathcal{P}} \mathbf{u}_{na} \mathbf{u}_{na}^T = \sum_{(n,a) \in \mathcal{P}} \lambda_{na} \mathbf{v}_{na} \mathbf{v}_{na}^T, \quad (8)$$

where \mathbf{u}_{na} is referred to as the *information vector*, given by

$$\mathbf{u}_{na} \triangleq \frac{\partial g(\theta_n|\theta_a)}{\partial \text{vec}(\Theta_{\mathcal{T}})} \sqrt{F_{na}} = \sqrt{\lambda_{na}} \mathbf{v}_{na}, \quad (9)$$

while $\sqrt{F_{na}} = \sqrt{\lambda_{na}}$ is the *information intensity* that captures the impact of the errors that the measurement r_{na} is subject to, and $\mathbf{v}_{na} \triangleq \frac{\partial g(\theta_n|\theta_a)}{\partial \text{vec}(\Theta_{\mathcal{T}})}$ being the *information gradient* that captures the impact of the type of measurement r_{na} , onto the FIM.

Proof: Let us start by noticing that given equations (5), (6) and (9), equation (7) can be rewritten as

$$\mathbf{F}_{\Theta_{\mathcal{T}}} = \mathbb{E} \left[\sum_{na} \sum_{ij} \mathbf{U}_{na}(r_{na}|\Theta_{\mathcal{T}}) \mathbf{U}_{ij}^T(r_{ij}|\Theta_{\mathcal{T}}) \right] \quad (10a)$$

$$= \sum_{na} \mathbb{E} [\mathbf{U}_{na}(r_{na}|\Theta_{\mathcal{T}}) \mathbf{U}_{na}^T(r_{na}|\Theta_{\mathcal{T}})] \quad (10b)$$

$$+ \underbrace{\sum_{\substack{na,ij \\ na \neq ij}} \mathbb{E} [\mathbf{U}_{na}(r_{na}|\Theta_{\mathcal{T}})]}_{=0} \underbrace{\mathbb{E} [\mathbf{U}_{ij}^T(r_{ij}|\Theta_{\mathcal{T}})]}_{=0}, \quad (10c)$$

where $\mathbf{U}_{na}(r_{na}|\Theta_{\mathcal{T}})$ is well-known as the *score function* [46] of the random variables r_{na} , which can be extracted from equation (7) and is defined as

$$\mathbf{U}_{na}(r_{na}|\Theta_{\mathcal{T}}) \triangleq \nabla_{\Theta_{\mathcal{T}}} \ln(p_{na}(r_{na}; g(\boldsymbol{\theta}_n|\boldsymbol{\theta}_a))), \quad (11)$$

and we have utilized the fact that for an unbiased estimator the score function has an expected value of zero [46].

Using the chain rule, the score function can be rewritten as

$$\mathbf{U}_{na}(r_{na}|\Theta_{\mathcal{T}}) = \frac{\partial \ln p_{na}(r_{na}; g(\boldsymbol{\theta}_n|\boldsymbol{\theta}_a))}{\partial g(\boldsymbol{\theta}_n|\boldsymbol{\theta}_a)} \frac{\partial g(\boldsymbol{\theta}_n|\boldsymbol{\theta}_a)}{\partial \Theta_{\mathcal{T}}}, \quad (12)$$

where the first partial derivative term of equation (12) is a scalar, while the second is a vector.

Combining equations (10c) and (12) yields

$$\mathbf{F}_{\Theta_{\mathcal{T}}} = \sum_{n=1}^{n_T} \sum_{a=1}^{n_A} \mathbb{E} \left[\left(\frac{\partial \ln p_{na}(r_{na}; g(\boldsymbol{\theta}_n|\boldsymbol{\theta}_a))}{\partial g(\boldsymbol{\theta}_n|\boldsymbol{\theta}_a)} \right)^2 \right] \times \frac{\partial g(\boldsymbol{\theta}_n|\boldsymbol{\theta}_a)}{\partial \Theta_{\mathcal{T}}} \frac{\partial g(\boldsymbol{\theta}_n|\boldsymbol{\theta}_a)^{\top}}{\partial \Theta_{\mathcal{T}}} \quad (13a)$$

$$= \sum_{n=1}^{n_T} \sum_{a=1}^{n_A} F_{na} \frac{\partial g(\boldsymbol{\theta}_n|\boldsymbol{\theta}_a)}{\partial \Theta_{\mathcal{T}}} \frac{\partial g(\boldsymbol{\theta}_n|\boldsymbol{\theta}_a)^{\top}}{\partial \Theta_{\mathcal{T}}}, \quad (13b)$$

$$= \sum_{n=1}^{n_T} \sum_{a=1}^{n_A} \mathbf{u}_{na} \mathbf{u}_{na}^{\top} = \sum_{n=1}^{n_T} \sum_{a=1}^{n_A} \lambda_{na} \mathbf{v}_{na} \mathbf{v}_{na}^{\top} \in \mathbb{R}^{\eta_{n_T} \times \eta_{n_T}}, \quad (13c)$$

where the quantity F_{na} is the Fisher information of the input r_{na} given in equation (5), while \mathbf{u}_{na} and \mathbf{v}_{na} are the information vector and the information gradient defined in the statement of Lemma 1. \square

Although evident from the proof itself, we emphasize that the equivalence between equations (7) and (8) is conditioned on the assumption of independence among the measurements in the input vector, and remark that such an assumption does not detract from the result, since it implies a maximization of the Fisher information [47], leading to a corresponding CRLB with the lowest possible values (*i.e.*, true fundamental limit). Finally, we highlight that in turn, the alternative FIM expression in equation (8) offers, beyond elegance, new insight by enabling easily access and assessment of the contribution of any given measurement r_{na} .

Examples for the information gradient \mathbf{v}_{na} and the information intensity λ_{na} for different types of measurements are given in Table I and Table II, and we emphasize that although the results of constructing the FIM using equations (7) and (13) are identical, the latter is a lot more convenient for extracting insight about the impact of each measurement on the FIM.

In particular, as pointed out already in [38], it is easy to study the consequence of removing the contribution of any given measurement r_{na} from the FIM constructed via equation (13), or investigate the impact of higher or smaller errors on any such variates.

In what follows, however, we take further advantage of the convenient structure of equation (13) to derive a FIM and latter the corresponding CRLB for RBL estimators, whereby the fundamental limit on the estimates not of individual landmark points, but rather of the overall location and orientation of the rigid body is of interest.

III. DERIVATION OF THE CRLB FOR RBL

As discussed in Subsection II-A, the objective of RBL algorithms [37], [40], [41] is to find the position, as determined by the translation vector \mathbf{t} , and the orientation, as determined by the yaw, pitch and roll angles α, β and γ , respectively, captured by the corresponding rotation matrix \mathbf{Q} , as described by equation (3) and illustrated in Figure 2. In order to assess the performance of RBL algorithms it is therefore relevant to obtain FIMs and corresponding CRLBs relative to the estimation parameters \mathbf{t} and \mathbf{Q} .

A. CRLB Formulation for the Translation Vector

Due to the independence among the elements of the translation vector, and among the yaw, pitch and roll angles, captured in the rotation matrix, the bounds for both parameters can be obtained individually. To that end, let us first consider the previously described RBL scenario and map the notation to what has been introduced in the construction of the FIM.

In particular, in a RBL scenario the target group $\Theta_{\mathcal{T}}$ can be defined as the positions of the transformed rigid body, as described before, such that equation (3) can be specifically rewritten as

$$\Theta_{\mathcal{T}} = \mathbf{Q} \cdot \mathbf{C}_1 + \mathbf{t} \cdot \mathbf{1}_{n_T}^{\top}, \quad (14)$$

which, for convenience, can be rewritten for the individual target point n as

$$\boldsymbol{\theta}_n = \mathbf{Q} \cdot \mathbf{c}_n + \mathbf{t}. \quad (15)$$

Following the information-centric construction method described earlier, the FIM for the translation vector \mathbf{t} (in three dimensions) is then given by

$$\begin{aligned} \mathbf{F}_{\mathbf{t}} &= \sum_{(n,a) \in \mathcal{P}} \lambda_{na} \mathbf{v}_{na} \mathbf{v}_{na}^{\top} \\ &= \sum_{(n,a) \in \mathcal{P}} \lambda_{na} \frac{\partial g(\boldsymbol{\theta}_n|\boldsymbol{\theta}_a)}{\partial \mathbf{t}} \left(\frac{\partial g(\boldsymbol{\theta}_n|\boldsymbol{\theta}_a)}{\partial \mathbf{t}} \right)^{\top} \in \mathbb{R}^{3 \times 3}. \end{aligned} \quad (16)$$

The information gradient associated with the dissimilarity function $g(\boldsymbol{\theta}_n|\boldsymbol{\theta}_a)$ w.r.t the translation vector \mathbf{t} in the latter equation can be obtained by using double dot product⁴, also known as the Frobenius inner product and the differential approach [48], [49]. As described in Appendix B, depending on the type of measurement, the information gradient changes

⁴Note that even though it seems intuitive to use the chain rule to decompose the gradient into two parts, namely a partial derivative of the dissimilarity function w.r.t the matrix of target coordinates $\Theta_{\mathcal{T}}$, and a partial derivative of $\Theta_{\mathcal{T}}$ w.r.t the translation vector \mathbf{t} , this concept cannot be applied directly, due to the mismatching sizes of the partial derivatives.

and thus, the FIM for the translation vector \mathbf{t} with respect to distance, angle of arrival (AoA) and angle difference of arrival (ADoA) measurements, collected in the sets \mathcal{P}_d , \mathcal{P}_ψ and $\mathcal{P}_{\psi'}$, respectively, can be expressed as

$$\begin{aligned} \mathbf{F}_t &= \sum_{(n,a) \in \mathcal{P}_d} \lambda_{na} g'|_t^d (g'|_t^d)^\top + \sum_{(n,a) \in \mathcal{P}_\psi} \lambda_{na} g'|_t^\psi (g'|_t^\psi)^\top \\ &+ \sum_{(n,a) \in \mathcal{P}_{\psi'}} \lambda_{na} g'|_t^{\psi'} (g'|_t^{\psi'})^\top \in \mathbb{R}^{\eta \times \eta}, \end{aligned} \quad (17)$$

where λ_{na} is the information intensity given in Table II and the variables $g'|_t^d$, $g'|_t^\psi$ and $g'|_t^{\psi'}$ denote the gradients of the dissimilarity function w.r.t the translation vector \mathbf{t} , for the distance, angle of arrival and angle difference of arrival measurements, respectively.

We emphasize the simplicity of the CRLB for the translation vector given by this expression compared to what one would obtain working directly with equation (7), which is a consequence of the information-centric approach to construct FIMs, as described in Subsection II-B, and the fact that translation vector \mathbf{t} is a coordinate vector similar to $\boldsymbol{\theta}_n$.

With the FIM in hand, the CRLB for the translation vector is a lower bound on the variance of any unbiased estimator, such that given a corresponding estimate $\hat{\mathbf{t}}$, we have [50]

$$\boldsymbol{\Omega}_t \triangleq \mathbb{E}[(\hat{\mathbf{t}} - \mathbf{t})(\hat{\mathbf{t}} - \mathbf{t})^\top] \succeq \mathbf{F}_t^{-1}. \quad (18)$$

In many cases, one is not interested in the positive-semidefinite inequality form of the CRLB given in equation (18), but on the CRLB for \mathbf{t} as whole, which is given by

$$\bar{\omega}_t \triangleq \frac{\text{tr}(\mathbf{F}_t^{-1})}{\eta}. \quad (19)$$

B. CRLB Formulation for the Rotation Matrix

While in some applications the yaw, pitch and roll angles α , β and γ are of interest, in the case of RBL the rotation matrix \mathbf{Q} is usually of interest, since instead of estimating the angles individually, the rotation matrix \mathbf{Q} can be estimated directly.

Following the same approach as before, the FIM for the rotation matrix \mathbf{Q} can be derived by using the differential approach the different dissimilarity functions $g(\boldsymbol{\theta}_n|\boldsymbol{\theta}_a)$ w.r.t the vectorized version rotation matrix $\text{vec}(\mathbf{Q})$, which leads to

$$\begin{aligned} \mathbf{F}_Q &= \sum_{(n,a) \in \mathcal{P}} \lambda_{na} \mathbf{v}_{na} \mathbf{v}_{na}^\top = \sum_{(n,a) \in \mathcal{P}} \lambda_{na} \frac{\partial g(\boldsymbol{\theta}_n|\boldsymbol{\theta}_a)}{\partial \text{vec}(\mathbf{Q})} \left(\frac{\partial g(\boldsymbol{\theta}_n|\boldsymbol{\theta}_a)}{\partial \text{vec}(\mathbf{Q})} \right)^\top \\ &= \sum_{(n,a) \in \mathcal{P}_d} \lambda_{na} g'|_Q^d (g'|_Q^d)^\top + \sum_{(n,a) \in \mathcal{P}_\psi} \lambda_{na} g'|_Q^\psi (g'|_Q^\psi)^\top \\ &+ \sum_{(n,a) \in \mathcal{P}_{\psi'}} \lambda_{na} g'|_Q^{\psi'} (g'|_Q^{\psi'})^\top \in \mathbb{R}^{\eta^2 \times \eta^2}, \end{aligned} \quad (20)$$

where the information intensity is defined as before, and the information gradients for the different types of measurements are derived in Appendix B.

Finally, given that the estimator of the rotation matrix $\hat{\mathbf{Q}}$ is unbiased, the covariance matrix corresponding to the unbiased estimate $\hat{\mathbf{Q}}$ is bounded by the CRLB [50]

$$\boldsymbol{\Omega}_Q \triangleq \mathbb{E}[(\hat{\mathbf{Q}} - \mathbf{Q})(\hat{\mathbf{Q}} - \mathbf{Q})^\top] \succeq \mathbf{F}_Q^{-1}. \quad (21)$$

The average CRLB for the rotation matrix \mathbf{Q} can be obtained by taking the trace of the inverse of the FIM and scaling by the dimension of it, which for the rotation matrix is η^2 , leading to

$$\bar{\omega}_Q = \frac{\text{tr}(\mathbf{F}_Q^{-1})}{\eta^2}. \quad (22)$$

However, while the formulation in equation (20) is valid for an arbitrary matrix of interest, this construction does not take into account the fact that the rotation matrix \mathbf{Q} is constrained since it belongs to the special orthogonal group, *i.e.*, $\mathbf{Q} \in \mathcal{SO}(\eta)$, satisfying the orthogonality condition $\mathbf{Q}^\top \mathbf{Q} = \mathbf{I}_\eta$ and the determinant condition $\det(\mathbf{Q}) = 1$. To mitigate this issue, the set of constraints in 3D space can be defined as

$$\begin{aligned} \mathbf{h}(\mathbf{Q}) &= \left[\|\mathbf{q}_1\|^2 - 1, \mathbf{q}_2^\top \mathbf{q}_1, \mathbf{q}_3^\top \mathbf{q}_1, \right. \\ &\left. \|\mathbf{q}_2\|^2 - 1, \mathbf{q}_2^\top \mathbf{q}_3, \|\mathbf{q}_3\|^2 - 1 \right]^\top = \mathbf{0}_6, \end{aligned} \quad (23)$$

where \mathbf{q}_1 , \mathbf{q}_2 and \mathbf{q}_3 are the columns of the rotation matrix \mathbf{Q} , and $\mathbf{0}_6$ is a zero vector of size 6×1 . Following [51], [52], the constraints can be incorporated into the FIM by defining the constraining matrix \mathbf{M} , which is given by

$$\mathbf{M} = \begin{bmatrix} -\mathbf{q}_3 & \mathbf{0}_3 & \mathbf{q}_2 \\ \mathbf{0}_3 & -\mathbf{q}_3 & -\mathbf{q}_1 \\ \mathbf{q}_1 & \mathbf{q}_2 & \mathbf{0}_3 \end{bmatrix} \in \mathbb{R}^{9 \times 3}, \quad (24)$$

such that $\mathbf{G}(\mathbf{Q})\mathbf{M} = \mathbf{0}$, where $[\mathbf{G}(\mathbf{Q})]_{i,j} = \partial[\mathbf{h}(\mathbf{Q})]_i / \partial[\mathbf{Q}]_j$. Finally, the constrained CRLB can be found by setting \mathbf{F}_Q such that

$$\bar{\omega}_Q^{(\text{CCRB})} = \mathbf{M} (\mathbf{M}^\top \mathbf{F}_Q \mathbf{M})^{-1} \mathbf{M}^\top. \quad (25)$$

The dissimilarity functions and corresponding information gradient vectors with respect to the translation vector \mathbf{t} and rotation matrix \mathbf{Q} derived in Appendix B are summarized in Table III.

C. CRLB Approximation: Relevance and Complexity Analysis

To avoid the matrix inversion in the calculation of the CRLB, an approximation can be used, as shown in Appendix C that leads to the approximated expression for the CRLB for the translation vector \mathbf{t} , given by

$$\bar{\omega}_t \approx \frac{\eta}{\text{tr}(\mathbf{F}_t)}, \quad (26)$$

which is shown for completion, but is not worthwhile, since the matrix inversion in equation (19) is not computationally expensive, and thus, the approximation is not needed.

Similar to the case of the translation vector, since the inverse of the FIM is computationally expensive to calculate, the same approximation of the CRLB, using the relation of the trace of the FIM and its inverse can be applied. Following the same approach as before, it can be shown that after the geometric-arithmetic mean inequality is applied, the following inequality can be found

$$\frac{\text{tr}(\mathbf{F}_Q^{-1})}{\eta^2} \leq \frac{\eta^2}{\text{tr}(\mathbf{F}_Q)}, \quad (27)$$

TABLE III
DISSIMILARITY FUNCTIONS AND INFORMATION GRADIENTS IN RBL LOCALIZATION SYSTEMS.

Measure Type	Dissimilarity Function $g(\theta_n \theta_a)$	Information Gradient $\frac{\partial g(\theta_n \theta_a)}{\partial \mathbf{t}}$	Information Gradient $\frac{\partial g(\theta_n \theta_a)}{\partial \text{vec}(\mathbf{Q})}$
Squared Distance	$\ \theta_n - \theta_a\ ^2 = d_{na}^2$	$2(\mathbf{Q}\mathbf{c}_t + \mathbf{t} - \theta_a)$	$2(\mathbf{c}_t \otimes \mathbf{I}_\eta)(\mathbf{Q}\mathbf{c}_t + \mathbf{t} - \theta_a)$
Angle of Arrival	$\text{acos}\left(\frac{\langle \mathbf{d}_{na}, \mathbf{b} \rangle}{\ \mathbf{d}_{na} - \langle \mathbf{d}_{na}, \mathbf{a} \rangle \mathbf{a}\ }\right)$	$-\frac{1}{\sqrt{1-x^2}} \cdot \left(\frac{(\mathbf{u}^\top \mathbf{P}\mathbf{u})\mathbf{b} - (\mathbf{u}^\top \mathbf{b}) \cdot \mathbf{P}\mathbf{u}}{\ \mathbf{P}\mathbf{u}\ ^3}\right)$	$-\frac{(\mathbf{c}_t \otimes \mathbf{I}_\eta)}{\sqrt{1-x^2}} \cdot \left(\frac{(\mathbf{u}^\top \mathbf{P}\mathbf{u})\mathbf{b} - (\mathbf{u}^\top \mathbf{b}) \cdot \mathbf{P}\mathbf{u}}{\ \mathbf{P}\mathbf{u}\ ^3}\right)$
Angle Difference of Arrival	$\text{acos}\left(\frac{d_{na}^2 + d_{ka}^2 - d_{nk}^2}{2d_{na}d_{ka}}\right)$	$-\frac{1}{\sqrt{1-x^2}} \cdot \left(\frac{\mathbf{u}}{2\ \mathbf{u}\ d} - \frac{\mathbf{u}d}{2\ \mathbf{u}\ ^3} + \frac{\ \mathbf{v}\ ^2\mathbf{u}}{2\ \mathbf{u}\ ^3d} - \frac{\mathbf{v}}{\ \mathbf{u}\ d}\right)$	$-\frac{(\mathbf{c}_t \otimes \mathbf{I}_\eta)}{\sqrt{1-x^2}} \cdot \left(\frac{\mathbf{u}}{2\ \mathbf{u}\ d} - \frac{\mathbf{u}d}{2\ \mathbf{u}\ ^3} + \frac{\ \mathbf{v}\ ^2\mathbf{u}}{2\ \mathbf{u}\ ^3d} - \frac{\mathbf{v}}{\ \mathbf{u}\ d}\right)$

* Note that the auxiliary variables \mathbf{u} , \mathbf{v} , \mathbf{P} and x are further defined in Appendix B for the sake of brevity of the expressions in the table.

TABLE IV
SIMULATION PARAMETERS

	Reference frames	Translations	Rotations	
$\mathbf{C}_1 =$	$\begin{bmatrix} -0.5 & 0.5 & 0.5 & -0.5 & -0.5 & 0.5 & -0.5 & 0.5 \\ -0.5 & -0.5 & 0.5 & 0.5 & -0.5 & -0.5 & 0.5 & 0.5 \\ -0.5 & -0.5 & -0.5 & -0.5 & 0.5 & 0.5 & 0.5 & 0.5 \end{bmatrix}$	$\in \mathbb{R}^{3 \times 8}$	$\mathbf{t}_1 = [-3, 0.5, 7]^\top$	$[\alpha_1, \beta_1, \gamma_1] = [10^\circ, 20^\circ, 45^\circ]$
$\mathbf{C}_2 =$	$\begin{bmatrix} -10 & 10 & 10 & -10 & -10 & 10 & -10 & 10 \\ -10 & -10 & 10 & 10 & -10 & -10 & 10 & 10 \\ -10 & -10 & -10 & -10 & 10 & 10 & 10 & 10 \end{bmatrix}$	$\in \mathbb{R}^{3 \times 8}$	$\mathbf{t}_2 = [0, 0, 0]^\top$	$[\alpha_2, \beta_2, \gamma_2] = [0^\circ, 0^\circ, 0^\circ]$

which leads to an average CRLB approximation of

$$\bar{\omega}_{\mathbf{Q}} \approx \frac{\eta^2}{\text{tr}(\mathbf{F}_{\mathbf{Q}})}. \quad (28)$$

We remark that these approximations can be used to simplify the mathematical formulation of algorithms aimed at improving the performance of RBL schemes by optimizing system parameters such as anchor locations and the types of measurements that they should collect. Notice that although techniques to do so in the case of point-target localization exits, *e.g.*, [53]–[56], these techniques are fundamentally limited to very specific scenarios and cannot be generalized to systems employing multiple types of input information, nor to the RBL problems. In contrast, the information-centric method here contributed and the approximations in equations (26) and (28) leave the possibility for the Frame-theoretical anchor placement optimization approach for point-target localization developed in [45] to be extended to RBL problems, which shall be addressed in a follow-up work.

In terms of computational complexity, the proposed approximation of the CRLB requires only the computation of the trace of the FIM, which has a computational complexity of $\mathcal{O}(l)$, where l is the dimension of the FIM, while the computation of the inverse of the FIM in the exact CRLB has a computational complexity of $\mathcal{O}(l^3)$, due to the matrix inversion operation. Thus, the proposed approximation significantly reduces the computational burden, especially for large-scale problems where the dimension of the FIM is high. Notice, however that, as shown in Figures 3 and 4, the performance gap between the exact and approximate solutions decreases as the dimension of the FIM increases. Consequently, although the approximation is computationally efficient, it does not offer a great advantage over the exact solution in the rigid body localization problem, where the dimension of the FIM is relatively small, it is still useful in scenarios where computational resources are limited and the dimension of the FIM is larger, which opens up future research directions and optimization problems.

IV. NUMERICAL RESULTS

In this section we provide simulation results illustrating the outcome of the proposed Cramér-Rao Lower Bound (CRLB) for the RBL problem, comparing them to SotA RBL methods. The bounds are calculated as the average CRLB in order to be represented as the position error bound (PEB), such that it can be compared to the root mean square error (RMSE) of the SotA translation vector \mathbf{t} and the rotation matrix \mathbf{Q} estimates. The used system parameters are described in Table IV, unless stated otherwise.

A. Complete and Incomplete Information

To compare the performance of the various SotA methods to the proposed bounds, in terms of translation vector and rotation matrix estimates, we consider the methods proposed in [37], [42] respectively, estimating the parameters by measuring zero mean Normal distributed distance measurements with variance σ^2 . To be precise, we compare the CRLB in terms of the exact representation and the approximation that does not require the inverse of the FIM. Additionally, for the rotation matrix, we also provide the constrained CRLB where the rotation matrix is orthogonal and has a determinant of 1, *i.e.*, $\mathbf{Q} \in \mathcal{SO}(3)$.

The first set of results is shown in Figure 3 and Figure 4, illustrating the performance of conventional distance-based RBL methods for complete and incomplete information, compared to the corresponding bounds. In Figure 3, the CRLB for the translation vector \mathbf{t} is shown as a function of the range error σ for the exact CRLB, the approximation of it, the multidimensional scaling (MDS) based method proposed in [57] as well as the bound for incomplete measurements, where only 80% of the possible measurements were observed, compared to the incomplete MDS based method, as well as a robust RBL method proposed in [42]. It can be observed that if all measurements are available the MDS-SotA performs well, but not close to the corresponding bound. While the incomplete version of the MDS-SotA converges to a poor

error floor, the robust method only performs slightly worse than the fully connected scenario, even when only 80% of the observations are available, still not very close to the bound, but closer than in the fully connected case.

Next, in Figure 4, the CRLB for the rotation matrix \mathbf{Q} is shown as a function of the range error σ for the exact unconstrained CRLB, the unconstrained approximation and the constrained CRLB, compared to the least squares solution of [37], as well as the scenario of incomplete observations, again comparing the bound to the robust method of [42]. It can be observed that the approximation of the unconstrained bound is very close to the exact bound, while the constrained CRLB is slightly lower than the unconstrained bound, which is expected since the constrained CRLB makes use of the orthogonality condition of the rotation matrix, which leads to a lower bound.

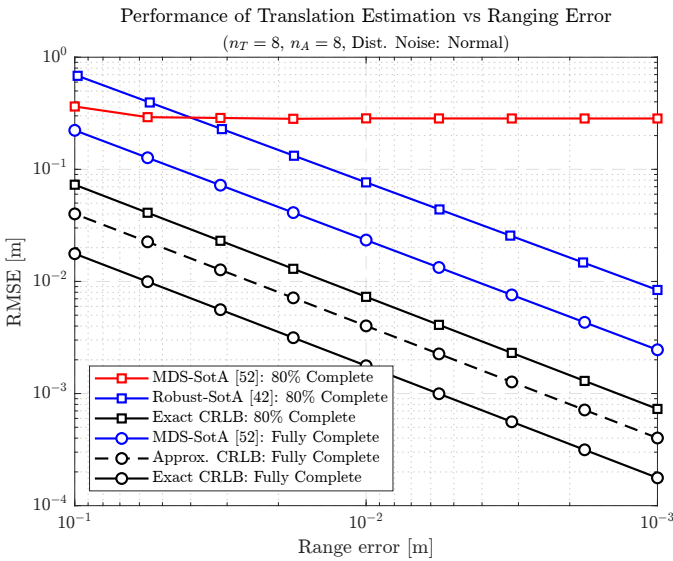


Fig. 3. RMSE of the translation vector estimate of the SotA and the CRLB variations, over the range error σ .

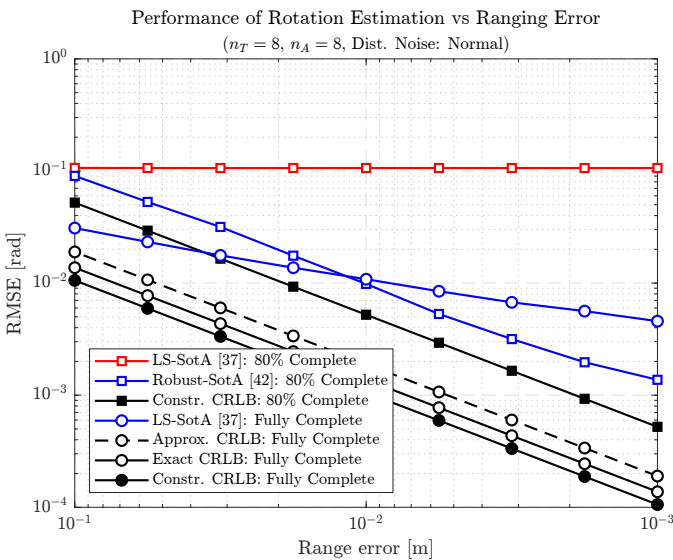


Fig. 4. RMSE of the rotation matrix estimate of the SotA and the CRLB variations, over the range error σ .

For the fully connected scenario, compared to the actual

estimate of the rotation matrix, especially in low error regimes, the CRLB is significantly lower, which hints at the potential that is left to improve the performance of the RBL methods, as well as the fact that only leveraging distance measurements is not optimal for rotation estimation. However, in the case of incomplete observations with 80% observed measurements, while the least square solution performs poorly at a high error floor, the robust method performs close to the corresponding bound for all error ranges, while outperforming the least square solution for lower error regimes.

All in all, it can be observed that for both, the translation and rotation, the estimates of most SotA methods are rather poor compared to the bound and that the bound degrades due to incomplete information, which indicates that there is still a lot of room for improvement, and the performance of the RBL methods can be improved significantly⁵. Nevertheless, as shown above, recent contributions already deal with scenarios of incomplete observations and can already get close to the CRLB for the rotation matrix estimate.

B. Evaluation with Heterogeneous Information

To showcase that the proposed CRLB framework is not limited to distance measurements, but can also be adopted to other types of measurements and specifically heterogeneous information, in this section we consider a RBL scenario where the measurements are a combination of distance and angle measurements, such that the rigid bod can be estimated by an super multidimensional scaling (SMDS)-based approach, presented in [58], calculating the bound with respect to the observed measurements between the nodes.

To that extend, consider a scenario, where the nodes perform not only distance measurements, but also AoA measurements, as shown in Figure 5. We therefore consider Gamma distributed distance measurements and Von-Mises distributed angle measurements, which illustrates the applicability of the bound to different types of measurements with different error distributions.

Figure 6 and 7 show the result of the translation and rotation estimation for an MDS-based approach, an SMDS-based approach, where the angles are obtained by using only the distance measurements, and a full SMDS approach, where both distance and angle measurements are used, compared to the corresponding CRLB, only with distance measurements and with both distance and angle measurements. It can be observed that the distance only SMDS approach is performing better than the MDS approach, which is expected since the SMDS approach uses more information, artificially created by estimating the angles, and thus, should lead to a better estimate. However, the distance only SMDS approach is not performing as well as the full SMDS approach, which is also expected, since the full SMDS approach uses both distance and angle measurements.

⁵While the performance of the RBL methods is closer to the CRLB for high range errors, the CRLB is not necessarily a good indicator of achievable accuracy in this regime due to its reliance on small-errors, which is the reason why we do not show the results for high range errors.

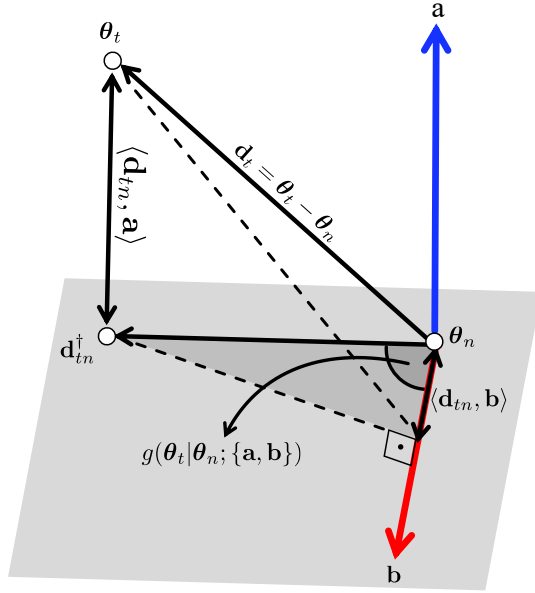


Fig. 5. Illustration of the angle-of-arrival measurements dissimilarity function calculation. Notice that the orthonormal vectors \mathbf{a} and \mathbf{b} are centered at θ_a , and act as a base for the angle of arrival measurement. Specifically, the plane onto which $\mathbf{d}_{n,a}$ is projected (giving \mathbf{d}_{tn}^\dagger) is defined by (normal to) \mathbf{a} and contains the reference vector \mathbf{b} against which the angle of arrival is measured.

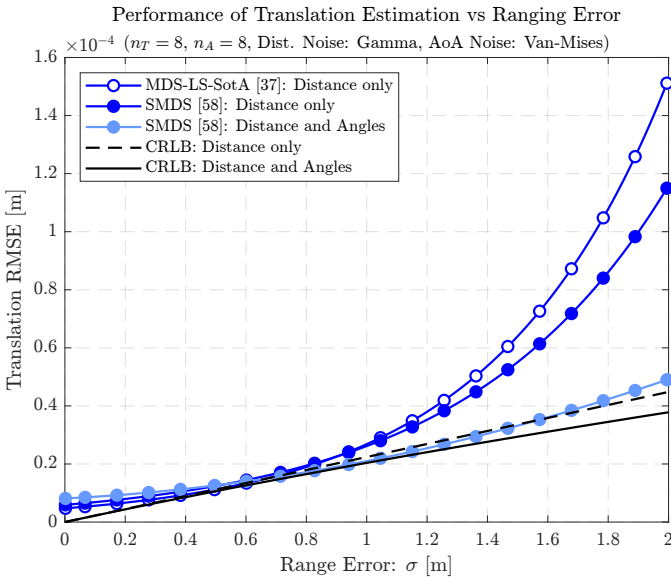


Fig. 6. RMSE of the translation vector estimate of the SotA and the CRLB variations, over various noise levels.

In Figure 6 it can be observed that in general, the full SMDS yields the best results with estimates close to the CRLB, while the SMDS approach with only distance measurements is performing better than the MDS approach, and slightly better than the full SMDS in small range error regimes, which is expected, since in [59] it was shown that the SMDS approach is not optimal in the small range error regime, and thus, the MDS approach performs better in this regime. Nevertheless, the distance only SMDS approach performs close to the CRLB in the small range error regime, which indicates that the SMDS approach is a good choice for the rigid body localization problem, even with only distance measurements.

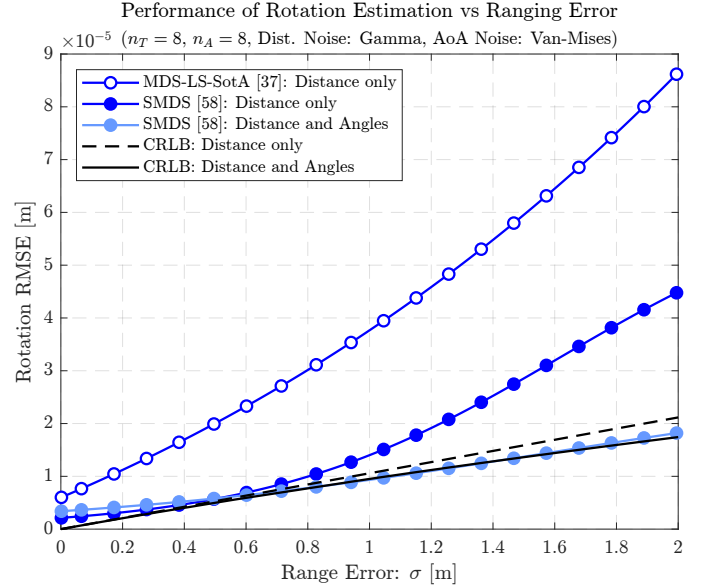


Fig. 7. RMSE of the rotation matrix estimate of the SotA and the CRLB variations, over various noise levels.

In Figure 7 similar properties can be observed, where the full SMDS approach is performing best, while the SMDS approach with only distance measurements is performing much better than the MDS approach, with the full SMDS approach is very close to the CRLB over the whole error range, while the SMDS approach with only distance measurements also performs close to the CRLB in the small range error regimes.

V. CONCLUSION

We proposed a novel information-centric framework for the construction of the CRLB for RBL, leading to a generalized CRLB for the rigid body parameters that includes the rotation matrix and translation vector applicable to any type of measurements. To that extend, first the classical element-centric FIM was presented and extended to the information-centric construction approach, leading to a generalized FIM framework that is applicable to arbitrary types of information and measurement error distributions and enables a straightforward adjustment of the bound when measurements are added or removed. Then the FIM was applied to the RBL problem, by making use of the information-gradient and information-intensity concepts, by exploiting the Frobenius inner product and the differential approach for derivatives, which lead to a generalized CRLB for the rigid body parameters. Furthermore, in addition to an approximate solution for the CRLB that does not require the inverse of the FIM, we also derived a constrained CRLB that ensures that the rotation matrix is orthogonal and has a determinant of 1, *i.e.*, $\mathbf{Q} \in \mathcal{SO}(3)$. Simulation results illustrate the great potential of RBL by using the proposed CRLB framework, showing that the proposed CRLB is a suitable bound for the RBL problem, not only in the case of distance measurements, but also in the case of heterogeneous information, such as a mixture of distance and angle-of-arrival measurements. However, comparing the bound to prior SotA methods, we show that the proposed CRLB is not tight in the low range error regimes for all SotA methods, and thus, further work on RBL estimators is needed to improve the performance of the estimation algorithms.

APPENDIX A

FISHER INFORMATION DERIVATIONS

As shown in Table II, the information intensity can be derived for different types of error statistics. As examples, in this section we derive the information intensities for Von-Mises [60], Nakagami [61], and Gamma variables, which can be directly plugged into the FIM construction framework.

A. Von Mises Variables

Let us start with the Von-Mises distribution (Tikhonov distribution) [60], which can be defined as

$$p(r_{na}; g(\boldsymbol{\theta}_n | \boldsymbol{\theta}_a)) = \frac{1}{2\pi I_0(\omega)} e^{\omega \cos(r_{na} - \mu)}, \quad (29)$$

where the variation function lies in the range of $-\pi \leq r_{na} \leq \pi$, while ω and μ are the shape and centrality parameters of the distribution and $I_0(x)$ denotes the modified Bessel function of the first kind and 0-th order [62].

From the above distribution, the corresponding Fisher information can be found according to equation (5), yielding

$$\begin{aligned} F &= \mathbb{E}_{r_{na}} \left[\left(\frac{\partial \ln p(r_{na}; g(\boldsymbol{\theta}_n | \boldsymbol{\theta}_a))}{\partial g(\boldsymbol{\theta}_n | \boldsymbol{\theta}_a)} \right)^2 \right] \\ &= \mathbb{E}_{r_{na}} \left[(-\omega \sin(r_{na} - \mu))^2 \right] = \omega^2 \mathbb{E}_{r_{na}} \left[\frac{1 - \cos(2(r_{na} - \mu))}{2} \right] \\ &= \frac{\omega^2}{2} - \int_{-\pi}^{\pi} \frac{\cos(2(r_{na} - \mu))}{2\pi I_0(\omega)} e^{\omega \cos(r_{na} - \mu)} dr_{na} = \frac{\omega^2}{2}, \quad (30) \end{aligned}$$

where we made use the geometric identity $\sin^2(x) = \frac{1 - \cos(2x)}{2}$ and the fact that $\cos(2x)$ and $\exp(\omega \cos(x))$ are two orthogonal functions for which the integral over $[0, 2\pi]$ vanishes, which leads to an information intensity of

$$\lambda = \sqrt{F} = \frac{\omega}{\sqrt{2}}. \quad (31)$$

B. Nakagami Variables

Next, the distribution of the Nakagami- m variable [61] can be investigated, where the corresponding PDF is defined as

$$p(r_{na}; g(\boldsymbol{\theta}_n | \boldsymbol{\theta}_a)) = \frac{2m^m}{\Gamma(m)\Upsilon^m} r_{na}^{2m-1} \exp\left(-\frac{m}{\Upsilon} r_{na}^2\right), \quad (32)$$

where $m = \Upsilon^2 / \mathbb{E}[(r_{na}^2 - \Upsilon)^2]$ is the shape parameter with $m \geq \frac{1}{2}$, $\Upsilon = \mathbb{E}[r_{na}^2] \geq 0$ is the second moment of the distribution that controls the spread and $\Gamma(\cdot)$ is the Gamma function [63].

Similarly to before, we follow equation (5), to define the FIM corresponding to the Nakagami- m distribution as

$$\begin{aligned} F &= \mathbb{E}_{r_{na}} \left[\left(\frac{\partial \ln p(r_{na}; g(\boldsymbol{\theta}_n | \boldsymbol{\theta}_a))}{\partial g(\boldsymbol{\theta}_n | \boldsymbol{\theta}_a)} \right)^2 \right] \\ &= \mathbb{E}_{r_{na}} \left[\left(\frac{2m-1}{r_{na}} - \frac{2mr_{na}}{\Upsilon} \right)^2 \right] \\ &= (2m-1)^2 \mathbb{E}_{r_{na}}[r_{na}^{-2}] + \frac{4m^2}{\Upsilon^2} \mathbb{E}_{r_{na}}[r_{na}^2] - \frac{8m^2-4m}{\Upsilon} \\ &= (2m-1)^2 \cdot \frac{m}{(m-1)\Upsilon} + \frac{4m^2}{\Upsilon^2} \cdot \Upsilon - \frac{8m^2-4m}{\Upsilon} \\ &= \frac{m(4m-3)}{\Upsilon(m-1)}, \quad (33) \end{aligned}$$

which leads to an information intensity of

$$\lambda = \sqrt{F} = \sqrt{\frac{m(4m-3)}{\Upsilon(m-1)}}. \quad (34)$$

In the above proof, to derive the first term of the expression, we used the general integral property [64, p361]

$$\int_0^\infty x^{\alpha-1} e^{-px^\mu} dx = \frac{1}{\mu} p^{-\alpha/\mu} \Gamma\left(\frac{\alpha}{\mu}\right), \quad (35)$$

while for the second term we employed the formula for the k -th moment of Nakagami distribution $\mathbb{E}[r_{na}^k] = \left(\frac{\Upsilon}{m}\right)^{\frac{k}{2}} \frac{\Gamma(m+k/2)}{\Gamma(m)}$ [61].

C. Gamma Variables

Finally, we can investigate information intensity of the Gamma distribution. Although there exists multiple parameterization of the Gamma distribution, we choose to use the one with the corresponding PDF given by

$$p(r_{na}; g(\boldsymbol{\theta}_n | \boldsymbol{\theta}_a)) = \frac{1}{\Gamma(\kappa)v^\kappa} r_{na}^{\kappa-1} \exp\left(-\frac{r_{na}}{v}\right), \quad (36)$$

where $\kappa > 0$ and $v > 0$ are the shape and scale parameter accordingly. Similar to the above sections and following equation (5), the FIM corresponding to Gamma distribution can be derived as

$$\begin{aligned} F &= \mathbb{E}_{r_{na}} \left[\left(\frac{\partial \ln p(r_{na}; g(\boldsymbol{\theta}_n | \boldsymbol{\theta}_a))}{\partial g(\boldsymbol{\theta}_n | \boldsymbol{\theta}_a)} \right)^2 \right] \\ &= \mathbb{E}_{r_{na}} \left[\left(\frac{\kappa-1}{r_{na}} - \frac{1}{v} \right)^2 \right] \\ &= (\kappa-1)^2 \mathbb{E}_{r_{na}}[r_{na}^{-2}] - \frac{2(\kappa-1)}{v} \mathbb{E}_{r_{na}}[r_{na}^{-1}] + \frac{1}{v^2} \\ &= (\kappa-1)^2 \cdot \frac{1}{v^2(\kappa-1)(\kappa-2)} - \frac{2(\kappa-1)}{v} \cdot \frac{1}{v(\kappa-1)} + \frac{1}{v^2} \\ &= \frac{1}{v^2(\kappa-2)}, \quad (37) \end{aligned}$$

with the information intensity given by

$$\lambda = \sqrt{F} = \sqrt{\frac{1}{v^2(\kappa-2)}}. \quad (38)$$

Again, in the above proof, to derive the first and second term of the expression, we used the general integral property from equation (35). APPENDIX B

GRADIENT DERIVATION FOR RIGID BODY PARAMETERS

To derive the gradient of the dissimilarity function with respect to the rigid body parameters, we consider the differential approach for matrix calculus [48], which allows us to compute the gradient of the dissimilarity function for different types of measurements, by using the properties of the double dot product. The double dot product, also known as the Frobenius inner product [49], is a way to compute the inner product of two matrices by treating them as vectors in a higher-dimensional space. For two $m \times n$ matrices \mathbf{A} and \mathbf{B} , the Frobenius inner product is defined as

$$\mathbf{A} : \mathbf{B} = \sum_{i=1}^m \sum_{j=1}^n \mathbf{A}_{ij} \mathbf{B}_{ij} = \text{tr}(\mathbf{A}^T \mathbf{B}), \quad (39)$$

where \mathbf{A}_{ij} and \mathbf{B}_{ij} are the elements of \mathbf{A} and \mathbf{B} , and tr denotes the trace (sum of diagonal elements). This is equivalent to the sum of the element-wise products or the trace of the matrix product $\mathbf{A}^\top \mathbf{B}$.

Similar to multiplication properties, the Frobenius inner product satisfies the commutative property $\mathbf{A} : \mathbf{B} = \mathbf{B} : \mathbf{A}$, the distributive property $\langle a\mathbf{A} + b\mathbf{C}, \mathbf{B} \rangle_F = a\langle \mathbf{A}, \mathbf{B} \rangle_F + b\langle \mathbf{C}, \mathbf{B} \rangle_F$, for scalars a, b and matrices $\mathbf{A}, \mathbf{C}, \mathbf{B}$, and specifically the following property to rearrange the matrices in the inner product $\mathbf{C}\mathbf{A} : \mathbf{B} = \mathbf{C} : \mathbf{B}\mathbf{A}^\top = \mathbf{A} : \mathbf{C}^\top \mathbf{B}$.

A. Square Distance Measurements

To begin, consider the dissimilarity function $g(\theta_n | \theta_a)$ defined as the squared Euclidean distance between two points in a rigid body localization scenario, where θ_n is the target position and θ_a is the anchor position, given by

$$g(\theta_n | \theta_a) = \|\theta_n - \theta_a\|^2. \quad (40)$$

To simplify the notation, let us denote an auxiliary variable $\mathbf{u} = \theta_n - \theta_a = \mathbf{Q}\mathbf{c}_t + \mathbf{t} - \theta_a$, such that the dissimilarity function can be rewritten as

$$g = \mathbf{u}^\top \mathbf{u} = \mathbf{u} : \mathbf{u}, \quad (41)$$

where $\mathbf{u} : \mathbf{u}$ denotes the double dot product of the vector \mathbf{u} with itself.

Next, the differential of the dissimilarity function with respect to \mathbf{u} can be computed as

$$dg = 2\mathbf{u} : d\mathbf{u}. \quad (42)$$

To obtain the gradient of the dissimilarity function with respect to the parameters of interest, we need to compute the differential $d\mathbf{u}$ for the two different cases, *i.e.*, translation and rotation. In the first case, we consider the translation of the target position, where the differential can be expressed as

$$d\mathbf{u} = d\mathbf{t}. \quad (43)$$

Following the rules of using the double dot product for gradients using differentials, we can insert the differential into the expression for the dissimilarity function, leading to

$$dg = 2\mathbf{u} : d\mathbf{t}, \quad (44)$$

which leads to the gradient of the dissimilarity function with respect to the translation vector \mathbf{t} as

$$g'_{|\mathbf{t}}^d = \frac{\partial g(\theta_n | \theta_a)}{\partial \mathbf{t}} = 2\mathbf{u} = 2(\mathbf{Q}\mathbf{c}_t + \mathbf{t} - \theta_a). \quad (45)$$

In the second case, we consider the vectorized rotation matrix $\text{vec}(\mathbf{Q})$, where first, the auxiliary variable \mathbf{u} can be rewritten as

$$\mathbf{u} = (\mathbf{c}_t^\top \otimes \mathbf{I}_\eta) \text{vec}(\mathbf{Q}) + \mathbf{t} - \theta_a, \quad (46)$$

with the corresponding differential given by

$$d\mathbf{u} = (\mathbf{c}_t^\top \otimes \mathbf{I}_\eta) d\text{vec}(\mathbf{Q}). \quad (47)$$

Finally, inserting the differential into the expression for the dissimilarity function, we obtain

$$dg = 2\mathbf{u} : (\mathbf{c}_t^\top \otimes \mathbf{I}_\eta) d\text{vec}(\mathbf{Q}), \quad (48)$$

which leads to the gradient of the dissimilarity function with respect to the vectorized rotation matrix $\text{vec}(\mathbf{Q})$ as

$$g'_{|\mathbf{Q}}^d = \frac{\partial g(\theta_n | \theta_a)}{\partial \text{vec}(\mathbf{Q})} = 2(\mathbf{c}_t \otimes \mathbf{I}_\eta)(\mathbf{Q}\mathbf{c}_t + \mathbf{t} - \theta_a). \quad (49)$$

B. Angle of arrival measurements

Next, the dissimilarity function for the angle of arrival (AoA) measurements is considered, which is defined as the angle between two vectors in a rigid body localization scenario, as illustrated in Figure 5. The dissimilarity function is given by $g(\theta_t | \theta_n, \mathbf{a}, \mathbf{b})$ is defined as

$$g(\theta_t | \theta_n, \mathbf{a}, \mathbf{b}) = \arccos\left(\frac{\langle \mathbf{d}_{na}, \mathbf{b} \rangle}{\|\mathbf{d}_{na} - \langle \mathbf{d}_{na}, \mathbf{a} \rangle \mathbf{a}\|}\right), \quad (50)$$

where again, an auxiliary variable can be defined as

$$\mathbf{u} = \mathbf{d}_{na} = \theta_n - \theta_a = \mathbf{Q}\mathbf{c}_t + \mathbf{t} - \theta_a, \quad (51)$$

such that the dissimilarity function can be rewritten as

$$g = \arccos\left(\frac{\mathbf{u}^\top \mathbf{b}}{\|\mathbf{u} - \mathbf{u}^\top \mathbf{a}\mathbf{a}\|}\right) = \arccos(x). \quad (52)$$

To avoid the chain rule, the differential approach enables the step by step computation of the differentials until the desired parameter is reached, such that the final gradient can be computed. Thus, to start with, the differential of the dissimilarity function with respect to x can be computed as

$$dg = -\frac{1}{\sqrt{1-x^2}} dx, \quad (53)$$

where the variable x is defined as

$$x = \frac{\mathbf{u}^\top \mathbf{b}}{\|\mathbf{u} - \mathbf{u}^\top \mathbf{a}\mathbf{a}\|} = \frac{\mathbf{b}}{\|\mathbf{u} - \mathbf{u}^\top \mathbf{a}\mathbf{a}\|} : \mathbf{u} = \frac{\mathbf{b}}{\|(\mathbf{I} - \mathbf{a}\mathbf{a}^\top)\mathbf{u}\|} : \mathbf{u}. \quad (54)$$

Next, the differential of x with respect to \mathbf{u} can be computed, where the projection matrix $\mathbf{P} = \mathbf{I} - \mathbf{a}\mathbf{a}^\top$ is used to simplify the expression, leading to

$$dx = \frac{(\mathbf{u}^\top \mathbf{P}\mathbf{u})\mathbf{b} - (\mathbf{u}^\top \mathbf{b}) \cdot \mathbf{P}\mathbf{u}}{(\|\mathbf{P}\mathbf{u}\|)^3} : d\mathbf{u}. \quad (55)$$

Inserting the differential into the expression for the dissimilarity function, we obtain

$$dg = -\frac{1}{\sqrt{1-x^2}} \cdot \underbrace{\left(\frac{(\mathbf{u}^\top \mathbf{P}\mathbf{u})\mathbf{b} - (\mathbf{u}^\top \mathbf{b}) \cdot \mathbf{P}\mathbf{u}}{(\|\mathbf{P}\mathbf{u}\|)^3}\right)}_{\mathbf{w} \in \mathbb{R}^{3 \times 1}} : d\mathbf{u}, \quad (56)$$

where again, the differential $d\mathbf{u}$ can be computed for the two different cases, *i.e.*, translation and rotation, as before. Thus, for the translation case, the differential expression for the dissimilarity function as

$$dg = -\frac{1}{\sqrt{1-x^2}} \cdot \mathbf{w} : d\mathbf{t}, \quad (57)$$

which leads to the gradient of the dissimilarity function with respect to the translation vector \mathbf{t} as

$$g'_{|\mathbf{t}}^\psi = \frac{\partial g(\theta_t | \theta_n, \mathbf{a}, \mathbf{b})}{\partial \mathbf{t}} = -\frac{1}{\sqrt{1-x^2}} \cdot \mathbf{w} \in \mathbb{R}^{3 \times 1}. \quad (58)$$

In the second case, for the rotation case, the differential expression for the dissimilarity function as

$$dg = -\frac{1}{\sqrt{1-x^2}} \cdot \mathbf{w} : (\mathbf{c}_t^\top \otimes \mathbf{I}_\eta) d\text{vec}(\mathbf{Q}), \quad (59)$$

which leads to the gradient of the dissimilarity function with respect to the vectorized rotation matrix $\text{vec}(\mathbf{Q})$ as

$$g'|\mathbf{Q}^\psi = \frac{\partial g(\boldsymbol{\theta}_t|\boldsymbol{\theta}_n, \mathbf{a}, \mathbf{b})}{\partial \text{vec}(\mathbf{Q})} = -\frac{(\mathbf{c}_t \otimes \mathbf{I}_\eta)}{\sqrt{1-x^2}} \cdot \mathbf{w} \in \mathbb{R}^{9 \times 1}. \quad (60)$$

C. Angle difference of arrival measurements

Finally, the dissimilarity function for the ADoA measurements $g(\boldsymbol{\theta}_n|\boldsymbol{\theta}_n, \boldsymbol{\theta}_k)$ is considered, given by

$$g(\boldsymbol{\theta}_n|\boldsymbol{\theta}_n, \boldsymbol{\theta}_k) = \arccos\left(\frac{d_{na}^2 + d_{ka}^2 - d_{nk}^2}{2d_{na}d_{ka}}\right), \quad (61)$$

where the distances are defined as

$$d_{na} = \|\boldsymbol{\theta}_n - \boldsymbol{\theta}_a\|, \quad (62a)$$

$$d_{nk} = \|\boldsymbol{\theta}_n - \boldsymbol{\theta}_k\|, \quad (62b)$$

$$d_{ka} = \|\boldsymbol{\theta}_k - \boldsymbol{\theta}_a\|, \quad (62c)$$

such that the auxiliary variables can be defined as

$$\mathbf{u} = \boldsymbol{\theta}_n - \boldsymbol{\theta}_a = \mathbf{Q}\mathbf{c}_t + \mathbf{t} - \boldsymbol{\theta}_a, \quad (63a)$$

$$\mathbf{v} = \boldsymbol{\theta}_n - \boldsymbol{\theta}_k = \mathbf{Q}\mathbf{c}_t + \mathbf{t} - \boldsymbol{\theta}_k, \quad (63b)$$

$$d = \|\boldsymbol{\theta}_k - \boldsymbol{\theta}_a\| = d_{ka}. \quad (63c)$$

Then, the dissimilarity function can be rewritten as

$$g = \arccos\left(\frac{\mathbf{u}^\top \mathbf{u} + d^2 + \mathbf{v}^\top \mathbf{v}}{2\|\mathbf{u}\|d}\right) = \arccos(x). \quad (64)$$

Since the dissimilarity function outer function, the arccos is identical to before, differential of with respect to x is also identical to equation (53). Next, the differential of x with respect to \mathbf{u} can be computed, where first, the variable x can be rewritten as

$$x = \frac{\mathbf{u}^\top \mathbf{u} + d^2 + \mathbf{v}^\top \mathbf{v}}{2\|\mathbf{u}\|d} = \frac{\mathbf{u}^\top \mathbf{u}}{2\|\mathbf{u}\|d} + \frac{d^2}{2\|\mathbf{u}\|d} + \frac{\mathbf{v}^\top \mathbf{v}}{2\|\mathbf{u}\|d}, \quad (65)$$

such that the differential of x with respect to \mathbf{u} can be computed as

$$dx = \frac{\mathbf{u}}{2\|\mathbf{u}\|d} : d\mathbf{u} - \frac{\mathbf{u}d}{2\|\mathbf{u}\|^3} : d\mathbf{u} + \frac{\|\mathbf{v}\|^2 \mathbf{u}}{2\|\mathbf{u}\|^3 d} : d\mathbf{u} - \frac{\mathbf{v}}{\|\mathbf{u}\|d} : d\mathbf{v}, \quad (66)$$

where in the last term the chain rule is used to compute the differential with respect to both \mathbf{u} and \mathbf{v} , since both auxiliary variables are dependent on the rigid body parameters. Nevertheless, the differential of these variables with respect to the rigid body parameters are identical, *i.e.* $d\mathbf{u} = d\mathbf{v}$, such that equation (66) can be rewritten as

$$dx = \left(\frac{\mathbf{u}}{2\|\mathbf{u}\|d} - \frac{\mathbf{u}d}{2\|\mathbf{u}\|^3} + \frac{\|\mathbf{v}\|^2 \mathbf{u}}{2\|\mathbf{u}\|^3 d} - \frac{\mathbf{v}}{\|\mathbf{u}\|d} \right) : d\mathbf{u}. \quad (67)$$

Next the differential of the dissimilarity function with respect to \mathbf{u} can be computed by inserting the differential of x into equation (53), leading to

$$dg = \frac{-1}{\sqrt{1-x^2}} \cdot \underbrace{\left(\frac{\mathbf{u}}{2\|\mathbf{u}\|d} - \frac{\mathbf{u}d}{2\|\mathbf{u}\|^3} + \frac{\|\mathbf{v}\|^2 \mathbf{u}}{2\|\mathbf{u}\|^3 d} - \frac{\mathbf{v}}{\|\mathbf{u}\|d} \right)}_{\mathbf{w} \in \mathbb{R}^{3 \times 1}} : d\mathbf{u}. \quad (68)$$

The final expression for the gradients are identical to the ones shown in equations (58) and (60), inserting the variables x and \mathbf{w} into the expression, leading to $g'|\mathbf{t}^{\psi'}$ and $g'|\mathbf{Q}^{\psi'}$ respectively.

APPENDIX C

LOW-COMPLEXITY APPROXIMATION OF CRLB

As mentioned before, since the inverse of the FIM is computationally expensive to calculate, we propose an approximation to the CRLB by using the relation of the trace of the FIM and its inverse, as already used in earlier SotA methods. Thus, consider the following pair of equations for the trace of the FIM and its inverse with respect to its eigenvalues Υ_i , such that

$$\text{tr}(\mathbf{F}) = \sum_{i=1}^{\eta} \Upsilon_i \triangleq T, \quad (69a)$$

$$\text{tr}(\mathbf{F}^{-1}) = \sum_{i=1}^{\eta} \frac{1}{\Upsilon_i}. \quad (69b)$$

Rewriting equations (69a) and (69b) it can be obtained that

$$\frac{1}{T} \sum_{i=1}^{\eta} \Upsilon_i = 1 \rightarrow \sum_{i=1}^{\eta} \frac{\Upsilon_i}{T} = 1 \rightarrow \sum_{i=1}^{\eta} \Upsilon'_i = 1 \quad (70)$$

Next, by using the geometric-arithmetic mean inequality, the following inequality can be found

$$\sum_{i=1}^{\eta} \frac{1}{\Upsilon'_i} \geq \eta \rightarrow \sum_{i=1}^{\eta} \frac{1}{\Upsilon_i} \geq \frac{\eta}{T}, \quad (71)$$

such that after combining the equations, the final relation can be found

$$\frac{\text{tr}(\mathbf{F}^{-1})}{\eta} \leq \frac{\eta}{\text{tr}(\mathbf{F})}, \quad (72)$$

which leads to an average CRLB approximation of

$$\bar{\omega} \approx \frac{\eta}{\text{tr}(\mathbf{F})}, \quad (73)$$

used to approximate the average CRLB for any parameter of interest, without the need to calculate the inverse of the FIM, where the nominator depends on the dimension of the FIM.

REFERENCES

- [1] R. Whiton, "Cellular localization for autonomous driving: A function pull approach to safety-critical wireless localization," *IEEE Vehicular Technology Magazine*, vol. 17, no. 4, pp. 28–37, 2022.
- [2] N. Correll *et al.*, *Introduction to autonomous robots: mechanisms, sensors, actuators, and algorithms*. Mit Press, 2022.
- [3] L. Baker *et al.*, "Localization and tracking of stationary users for augmented reality," *The Visual Computer*, vol. 40, no. 1, pp. 227–244, 2024.
- [4] Z. Wang *et al.*, "Intelligent vehicle self-localization based on double-layer features and multilayer LIDAR," *IEEE Transactions on Intelligent Vehicles*, vol. 5, no. 4, pp. 616–625, 2020.
- [5] S. Manickam *et al.*, "Unlocking the potential of digital twins: A comprehensive review of concepts, frameworks, and industrial applications," *IEEE Access*, vol. 11, pp. 135 147–135 158, 2023.
- [6] C. R. Rao, "Information and the accuracy attainable in the estimation of statistical parameters," in *Breakthroughs in Statistics: Foundations and basic theory*. Springer, 1992, pp. 235–247.
- [7] S. Gezici, "A survey on wireless position estimation," *Wireless Personal Communications*, vol. 44, no. 3, pp. 263–282, Feb 2008. [Online]. Available: <https://doi.org/10.1007/s11277-007-9375-z>

- [8] Q. Bader, S. Saleh, and A. Noureldin, "CRLB-based data-driven covariance tuning for 5G KF vehicular tracking," in *GLOBECOM 2024 - 2024 IEEE Global Communications Conference*, 2024, pp. 289–294.
- [9] K. R. R. Ranasinghe *et al.*, "Fast and efficient sequential radar parameter estimation in MIMO-OTFS systems," in *IEEE International Conference on Acoustics, Speech and Signal Processing (ICASSP)*, 2024.
- [10] K. Meng and C. Masouros, "Cooperative sensing and communication for ISAC networks: Performance analysis and optimization," in *2024 IEEE 25th International Workshop on Signal Processing Advances in Wireless Communications (SPAWC)*, 2024, pp. 446–450.
- [11] A. Bhattacharyya, "On some analogues of the amount of information and their use in statistical estimation (contd.)," *Sankhya: The Indian Journal of Statistics (1933-1960)*, vol. 8, no. 3, pp. 201–218, 1947.
- [12] D. A. S. Fraser, "Sufficient statistics and selection depending on the parameter," *The Annals of Mathematical Statistics*, vol. 23, no. 3, pp. 417–425, September 1952.
- [13] L. Weiss and A. Weinstein, "On the cramer-rao bound for the estimation of multidimensional parameters," *IEEE Transactions on Information Theory*, vol. 26, no. 5, pp. 624–626, 1980.
- [14] D. Burghal *et al.*, "A comprehensive survey of machine learning based localization with wireless signals," 2020.
- [15] H. Obeidat *et al.*, "A review of indoor localization techniques and wireless technologies," *Wireless Personal Communications*, vol. 119, pp. 289–327, 2021.
- [16] X. Shan *et al.*, "A survey of vehicle localization: Performance analysis and challenges," *IEEE Access*, vol. 11, pp. 107085–107107, 2023.
- [17] Z. Wang *et al.*, "Location awareness in beyond 5G networks via reconfigurable intelligent surfaces," *IEEE Journal on Selected Areas in Communications*, vol. 40, no. 7, pp. 2011–2025, 2022.
- [18] ITU-R, International Telecommunication Union - Radiocommunication Sector, "M.2160-0: Framework and overall objectives of the future development of IMT for 2030 and beyond," Nov. 2023.
- [19] J. A. Zhang *et al.*, "An overview of signal processing techniques for joint communication and radar sensing," *IEEE Journal of Selected Topics in Signal Processing*, vol. 15, no. 6, pp. 1295–1315, 2021.
- [20] H. S. Rou *et al.*, "From orthogonal time–frequency space to affine frequency-division multiplexing: A comparative study of next-generation waveforms for integrated sensing and communications in doubly dispersive channels," *IEEE Signal Processing Magazine*, vol. 41, no. 5, pp. 71–86, 2024.
- [21] K. R. R. Ranasinghe *et al.*, "Joint channel, data, and radar parameter estimation for AFDM systems in doubly-dispersive channels," *IEEE Transactions on Wireless Communications*, vol. 24, no. 2, pp. 1602–1619, 2025.
- [22] Y. Wang *et al.*, "An investigation and solution of angle based rigid body localization," *IEEE Transactions on Signal Processing*, vol. 68, pp. 5457–5472, 2020.
- [23] N. Führling *et al.*, "Soft-connected rigid body localization: State-of-the-art and research directions for 6G," 2023.
- [24] —, "Enabling next-generation V2X perception: Wireless rigid body localization and tracking," 2024. [Online]. Available: <https://arxiv.org/abs/2408.00349>
- [25] Q. Yu *et al.*, "Cooperative multi-rigid-body localization in wireless sensor networks using range and doppler measurements," *IEEE Internet of Things Journal*, pp. 1–1, 2023.
- [26] L. Zha *et al.*, "3D moving rigid body localization in the presence of anchor position errors," in *2021 International Symposium on Electrical, Electronics and Information Engineering*, ser. ISEIEE 2021. New York, NY, USA: Association for Computing Machinery, pp. 28–32., 2021
- [27] X. Dong *et al.*, "Rigid body localization in unsynchronized sensor networks: Analysis and solution," *IEEE Transactions on Wireless Communications*, pp. 1–1, 2023.
- [28] S. P. Chepuri *et al.*, "Rigid body localization using sensor networks," *IEEE Transactions on Signal Processing*, vol. 62, no. 18, pp. 4911–4924, 2014.
- [29] B. Zhou *et al.*, "Accurate rigid body localization using DoA measurements from a single base station," *Electronics*, 2019.
- [30] D.-R. Emenonye *et al.*, "Fundamentals of LEO-based localization," *IEEE Transactions on Information Theory*, vol. 71, no. 7, pp. 5277–5311, 2025.
- [31] A. A. D'Amico *et al.*, "Cramér–rao bounds for holographic positioning," *IEEE Transactions on Signal Processing*, vol. 70, pp. 5518–5532, 2022.
- [32] Y. Chen *et al.*, "Cramér–rao bounds and optimal design metrics for pose-graph slam," *IEEE Transactions on Robotics*, vol. 37, no. 2, pp. 627–641, 2021.
- [33] M. Angjelichinoski *et al.*, "Cramér–rao lower bounds of rss-based localization with anchor position uncertainty," *IEEE Transactions on Information Theory*, vol. 61, no. 5, pp. 2807–2834, 2015.
- [34] J. He *et al.*, "Cramér–rao lower bound analysis for elliptic localization with random sensor placements," *IEEE Transactions on Aerospace and Electronic Systems*, vol. 60, no. 4, pp. 5587–5595, 2024.
- [35] Y. Shen and M. Z. Win, "Fundamental limits of wideband localization—part I: A general framework," *IEEE Transactions on Information Theory*, vol. 56, no. 10, pp. 4956–4980, 2010.
- [36] Y. Shen *et al.*, "Fundamental limits of wideband localization—part II: Cooperative networks," *IEEE Transactions on Information Theory*, vol. 56, no. 10, pp. 4981–5000, 2010.
- [37] S. Chen and K. C. Ho, "Accurate localization of a rigid body using multiple sensors and landmarks," *IEEE Transactions on Signal Processing*, vol. 63, no. 24, pp. 6459–6472, 2015.
- [38] A. Ghods *et al.*, "On the structural nature of cooperation in distributed network localization," in *2014 48th Asilomar Conference on Signals, Systems and Computers*, 2014, pp. 1194–1198.
- [39] J. Diebel, "Representing attitude : Euler angles, unit quaternions, and rotation vectors," 2006.
- [40] V. Vitziv *et al.*, "Belief propagation-based rotation and translation estimation for rigid body localization," in *IEEE Wireless Communications and Networking Conference (WCNC)*, 2025, pp. 1–6.
- [41] N. Führling *et al.*, "6D rigid body localization and velocity estimation via gaussian belief propagation," *IEEE Transactions on Signal Processing*, vol. 73, pp. 3902–3917, 2025.
- [42] N. Führling *et al.*, "Robust egoistic rigid body localization," *IEEE Transactions on Signal Processing*, vol. 73, pp. 5076–5089, 2025.
- [43] N. Patwari *et al.*, "Relative location estimation in wireless sensor networks," *IEEE Transactions on Signal Processing*, vol. 51, no. 8, pp. 2137–2148, 2003.
- [44] T. Jia and R. M. Buehrer, "A new cramer-rao lower bound for TOA-based localization," in *MILCOM 2008 - 2008 IEEE Military Communications Conference*, 2008, pp. 1–5.
- [45] S. Van de Velde *et al.*, "Frame theory and optimal anchor geometries in wireless localization," in *2014 IEEE 79th Vehicular Technology Conference (VTC Spring)*, 2014, pp. 1–6.
- [46] D. R. Cox and D. V. Hinkley, *Theoretical Statistics*. Chapman and Hall/CRC, 1979.
- [47] S. M. Kay, *Fundamentals of Statistical Signal Processing: Estimation Theory*. Englewood Cliffs, New Jersey: Prentice Hall Signal Processing Series, 1993, vol. I.
- [48] J. R. Magnus and H. Neudecker, *Matrix differential calculus with applications in statistics and econometrics*. John Wiley & Sons, 2019.
- [49] R. Herzog *et al.*, "Metric frobenius norms and inner products of matrices and linear maps," *Linear Algebra and its Applications*, vol. 727, pp. 112–128, 2025.
- [50] S. M. Kay, *Fundamentals of Statistical Signal Processing, Volume 2: Detection Theory*. Upper Saddle River, NJ, USA: Prentice Hall PTR, 1998.
- [51] P. Stoica and B. C. Ng, "On the cramer-rao bound under parametric constraints," *IEEE Signal Processing Letters*, vol. 5, no. 7, pp. 177–179, 1998.
- [52] M. A. Nazari *et al.*, "mmWave 6D radio localization with a snapshot observation from a single BS," *IEEE Transactions on Vehicular Technology*, vol. 72, no. 7, pp. 8914–8928, 2023.
- [53] S. Xu and K. Dogançay, "Optimal sensor placement for 3-D angle-of-arrival target localization," *IEEE Transactions on Aerospace and Electronic Systems*, vol. 53, no. 3, pp. 1196–1211, 2017.
- [54] N. Saeed *et al.*, "Outlier detection and optimal anchor placement for 3-D underwater optical wireless sensor network localization," *IEEE Transactions on Communications*, vol. 67, no. 1, pp. 611–622, 2019.
- [55] M. Sadeghi *et al.*, "Optimal sensor placement for 2-D range-only target localization in constrained sensor geometry," *IEEE Transactions on Signal Processing*, vol. 68, pp. 2316–2327, 2020.
- [56] C. Ozturk and S. Gezici, "Anchor placement in TOA based wireless localization networks via convex relaxation," in *2021 IEEE International Black Sea Conference on Communications and Networking (BlackSeaCom)*, 2021, pp. 1–6.
- [57] N. Führling *et al.*, "Egoistic MDS-based rigid body localization," in *IEEE Wireless Communications and Networking Conference (WCNC)*, 2025, pp. 1–6.
- [58] N. Führling *et al.*, "SMDS-based Rigid Body Localization," in *IEEE International Conference on Computing, Networking and Communications (ICNC)*, 2026, pp. 1–6. (to appear)
- [59] G. T. F. de Abreu and G. Destino, "Super MDS: Source location from distance and angle information," in *2007 IEEE Wireless Communications and Networking Conference*, 2007, pp. 4430–4434.
- [60] G. T. de Abreu, "On the generation of Tikhonov variates," *IEEE Transactions on Communications*, vol. 56, no. 7, pp. 1157–1168, 2008.
- [61] N. Wang *et al.*, "Generalized method of moments estimation of the Nakagami-m fading parameter," *IEEE Transactions on Wireless Communications*, vol. 11, no. 9, pp. 3316–3325, 2012.
- [62] F. Bowman, *Introduction to Bessel functions*. Courier Corporation, 2012.
- [63] M. Abramowitz and I. A. Stegun, *Handbook of mathematical functions: with formulas, graphs, and mathematical tables*. Courier Corporation, 1965, vol. 55.
- [64] D. Z. A. Jeffrey, *Table of Integrals, Series, and Products*, 6th ed. Academic Press Inc., 2000.